

The delusive accuracy of global irrigation water withdrawal estimates

Supplementary Materials

Arnald Puy^{*1,2}, Razi Sheikholeslami³, Hoshin V. Gupta⁴, Jim W. Hall³,
Bruce Lankford⁵, Samuele Lo Piano⁶, Jonas Meier⁷, Florian Pappenberger⁸,
Amilcare Porporato⁹, Giulia Vico¹⁰, and Andrea Saltelli¹¹

¹ *Department of Ecology and Evolutionary Biology, M31 Guyot Hall, Princeton University, New Jersey 08544, USA. E-Mail: apuy@princeton.edu*

² *Centre for the Study of the Sciences and the Humanities (SVT), University of Bergen, Parkveien 9, PB 7805, 5020 Bergen, Norway.*

³ *Environmental Change Institute, School of Geography and the Environment, University of Oxford, Oxford, UK.*

⁴ *Department of Hydrology and Atmospheric Sciences, 1133 E. James E. Rogers Way, University of Arizona, Tucson AZ, USA.*

⁵ *School of International Development, University of East Anglia, Norwich, NR4 7TJ, United Kingdom*

⁶ *University of Reading, School of the Built Environment, JJ Thompson Building, Whiteknights Campus, Reading, RG6 6AF, United Kingdom*

⁷ *German Aerospace Center (DLR), German Remote Sensing Center (DFD), Münchner Strasse 20, 82234 Oberpfaffenhofen, Germany*

⁸ *European Centre for Medium-Range Weather Forecasts. Reading, UK / Bologna, Italy*

⁹ *Department of Civil and Environmental Engineering and Princeton High Meadows Environmental Institute, Princeton University, New Jersey, 08544, USA.*

¹⁰ *Department of Crop Production Ecology, Swedish University of Agricultural Sciences, Uppsala, SE-750 07, Sweden.*

¹¹ *Open Evidence Research, Universitat Oberta de Catalunya, Carrer Pujades 51-55, B45, 08005 Barcelona, Spain.*

*Corresponding author

Table of Contents

1	Calculation of irrigation water withdrawals	3
1.1	Irrigated areas	4
1.2	Crop evapotranspiration	4
1.3	Irrigation efficiency	8
2	Uncertainty and sensitivity analysis	11
2.1	Variance-based sensitivity analysis	11
2.2	Practical implementation	14
2.3	Assessment of uncertainties in the GHM literature	15
2.4	One-at-a-time (OAT) approach	17
2.5	Uncertainty and sensitivity analysis at the grid cell level	17
	References	22

1 Calculation of irrigation water withdrawals

In general, many large-scale hydrological models compute irrigation water withdrawals at a pre-determined spatio-temporal resolution with variations of the following equation [1, 2]:

$$y = \frac{I_a(ET_c - P)}{E_p} \quad (1)$$

where y is a scalar representing irrigation water withdrawals [m^3], I_a is the extension of irrigation [m^2], ET_c is the crop evapotranspiration [m], P is the precipitation [m] and E_p is the irrigation efficiency [-].

Equation 1 is based on a simple soil water budget extended to the irrigated area. Inputs to the soil water budget are represented by precipitation P and irrigation I , which in turn is the irrigation withdrawal, but reduced due the non-unitary efficiency E_p , i.e., $I = yE_p$. The only losses occur via the evapotranspiration ET_c which, as discussed below, corresponds to the crop needs under well-watered conditions.

As such, Equation 1 neglects the following phenomenons:

1. Canopy interception of precipitation, which reduces the precipitation that effectively recharges the soil water store. Using precipitation above the canopy leads to an overestimate of water made available to the crop via precipitation and hence an underestimate of water needs for irrigation. Canopy interception increases during the growing season as crop develops and the canopy closes. It also depends on the canopy architecture and, more importantly, on precipitation intensity, with larger fractions of precipitation intercepted (and evaporated directly from the canopy) for less intense and smaller precipitation events.
2. Losses via surface runoff and percolation below the rooting zone. This overestimates the soil water recharge via precipitation and hence underestimates irrigation requirements. Runoff is particularly relevant when precipitation events are intense and exceed the soil infiltration rate or soils are nearly saturated. Deep percolation is most relevant for wetter soils characterized by a coarser texture and low clay and soil carbon contents, when soil hydraulic conductivity becomes larger.
3. Changes in soil water storage in the rooting zone. This can have opposite effects on the estimated irrigation withdrawals, depending on the sign of this change in storage during the time period to which Equation 1 is applied. Yet, considering a rooting zone typical for crops [3] and a realistic soil porosity, the change in soil water storage can be as high as 200 mm, i.e., be comparable with growing season precipitation inputs in many locations.

This term becomes negligible only when the terms in Equation 1 are interpreted as integrals over periods of few years, during which changes in soil water storage are generally negligible. If Equation 1 is applied over single growing seasons, in regions prone to dry conditions and in need of irrigation, it can be expected that the change in soil water storage is negative over the growing season, i.e., soil are recharged in the off season and the stored water is used as additional source during the growing season.

In this case, neglecting the change in soil water storage leads to an overestimation of irrigation water withdrawals, because this extra amount of water is not considered.

Whether this potential overestimation in y counterbalances the underestimation stemming from neglecting canopy interception and losses via runoff and deep percolation depends primarily on the time scale at which the terms in Equation 1 are interpreted, soil features, plant water use and climatic conditions. Even considering these assumptions realistic, each term in Equation 1 has inherent uncertainties, as discussed in the Comment.

1.1 Irrigated areas

Currently, there are at least four different spatially-distributed maps informing on the extension of irrigation:

1. The Global Map of Irrigated Areas (FAO-GMIA) [4].
2. The Global Irrigation Area Map of the International Water Management Institute (IWMI-GIAM) [5].
3. The Global Rain-fed, Irrigated and Paddy Croplands Map (GRIPC) [6].
4. The map by Meier *et al.* [7].

These maps differ on the weight given to official statistics of irrigated areas and on the use of remote-sensing products, aerial imagery and historical maps. Figure S1 shows the extent to which they provide different extensions of irrigation for the same irrigated areas, e.g. for the same coordinates.

There are also two more datasets providing country-based estimates of the extension of irrigation:

1. AQUASTAT [8].
2. FAOSTAT [9].

Figures S2–S3 display the differences between the irrigated areas reported at the country level by all six resources mentioned above.

1.2 Crop evapotranspiration

The crop evapotranspiration is usually calculated as

$$ET_c = ET_0 k_c, \quad (2)$$

where ET_0 [mm]) is the reference crop evapotranspiration (usually grass or alfalfa) and k_c [-] is a coefficient that accounts for the differences between ET_0 and the crop under study.

In the Comment we focus on two ET_0 formulae, the most used by large-scale hydrological models: the Priestley-Taylor and the FAO-56 Penman Monteith [11]. In the case of the former, we have

$$ET_0 = \alpha \frac{\Delta A}{\Delta + \gamma}, \quad (3)$$

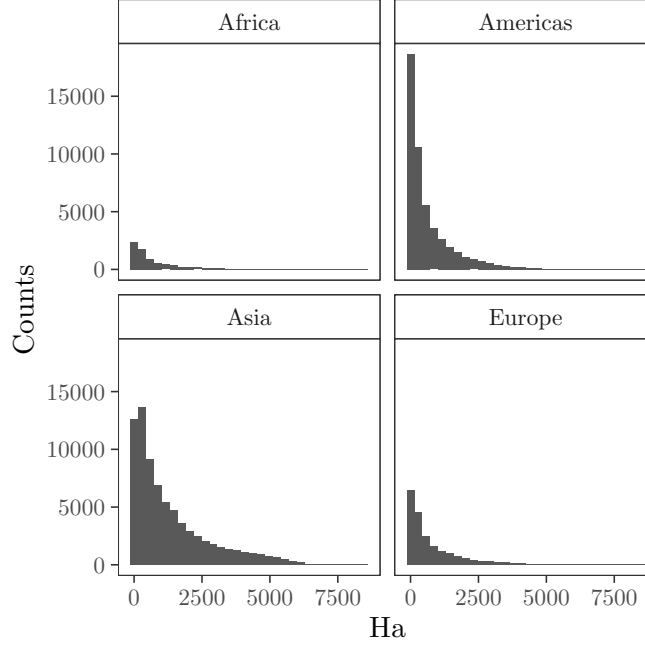


Figure S1: Distributions of the absolute difference between the irrigated areas reported by the GRIPC [6] and the FAO-GMIA [10] for the same exact coordinates (the same grid cells).

whereas for the latter, we have

$$ET_0 = \frac{0.408\Delta A + \gamma \frac{900}{T_a + 273} wv}{\Delta + \gamma(1 + 0.34w)}, \quad (4)$$

where A is the net radiation minus the soil heat flux ($\text{MJ m}^{-2} \text{d}^{-1}$), Δ is the gradient of saturated vapour pressure ($\text{kPa } ^\circ\text{C}^{-1}$), γ is the psychrometric constant ($\text{kPa } ^\circ\text{C}^{-1}$), α is the Priestley-Taylor constant, T_a is the mean daily air temperature at 2m ($^\circ\text{C}$), w is the average daily wind speed at 2m (m s^{-1}) and v is the vapor pressure deficit (kPa). See Allen *et al.* [12] for an explanation of the coefficients.

We rely on the work by Nichols *et al.* [13] to characterize the uncertainty in the parameters of Equations 3 and 4 (Table S1). See section 2.1 for the technical details of the uncertainty and sensitivity analysis conducted.

The results are shown in Figure S4. In Figure S4a–b we display the output of a global uncertainty and sensitivity analysis on ET_0 . The use of the Penman-Monteith results in $ET_0 = [126, 170]$ mm, whereas the use of the Priestley-Taylor’s results in $ET_0 = [265, 433]$ mm. ET_0 values can therefore vary by as much as 400% depending on the equation selected and by up to 90% if a specific equation (e.g., the Priestley Taylor) is adopted. This result aligns with previous studies suggesting that structural uncertainties may be more relevant than parametric uncertainties in the estimation of ET_0 [14]. In this example, all of the uncertainty in the FAO-56 Penman-Monteith equation is due to imprecision in the knowl-



Figure S2: Irrigated area estimates produced for Africa and the Americas by the FAO-GMIA [10], the IWM-GIAM [5], the GRIPC [6], Meier’s map [7], Aquastat [8] and FAOSTAT [9]. The data has been retrieved from Meier *et al.* [7].

edge of A , while in the case of the Priestley-Taylor equation, A and α are responsible for approximately 70% and 30% of the variance in ET_0 (Figure S4b).



Figure S3: Irrigated area estimates produced for Asia and Europe by the FAO-GMIA [10], the IWMI-GIAM [5], the GRIPC [6], Meier’s map [7], Aquastat [8] and FAOSTAT [9]. The data has been retrieved from Meier *et al.* [7].

If uncertainties in k_c are added to those in ET_0 to compute ET_c (Equation 2), we get an uncertainty cascade [15, 16]: the variance in k_c affects ET_0 and spills over to ET_c .

Table S1: Summary of the uncertainty in the parameters of the Priestley-Taylor and the FAO-56 Penman-Monteith Equations as proposed by Nichols *et al.* [13, Table 2] for the measurements conducted in the Bosque del Apache region, in New Mexico. A mid-morning day in June is taken as a typical day.

Input	Description	Distribution
α	Priestley-Taylor constant	$\mathcal{U}(1.134, 1.385)$
Δ	Vapour pressure	$\mathcal{U}(0.208, 0.211)$
γ	Psychrometric constant	$\mathcal{U}(0.058, 0.059)$
A	Net radiation minus soil heat flux	$\mathcal{U}(297.550, 402.448)$
T_a	Mean air temperature	$\mathcal{U}(26.730, 27.269)$
w	Wind speed at 3 m	$\mathcal{U}(2.375, 2.624)$
v	Vapour deficit	$\mathcal{U}(2.390, 2.589)$

Note how the distribution of ET_c values (Figure S4c) becomes much wider than that of ET_0 (Figure S4a), spanning almost one order of magnitude regardless of the ET_0 method selected and with the upper end having values larger than the lowest by a factor of 20 (Figure S4c). In this case, almost all the uncertainty is conveyed by k_c , while α and A turn from influential to almost non-influential (Figure S4d).

1.3 Irrigation efficiency

The engineering notion of “irrigation efficiency” discussed in the Comment is embedded in the E_p values produced by Döll & Siebert [2] and Rohwer *et al.* [17], which are used by many large-scale hydrological models. These values are accurate down to the third-digit and, according to the authors, are grounded on the empirical work conducted by Solley *et al.* [18, pp. 32–35] in USA, by Guera *et al.* [19, p. 5] in Asia, by FAO [20] in Africa or by Bos & Nugteren [21, pp. 20–22] at the irrigation system level.

Yet a detailed examination of the underlying data reveals that Döll & Siebert [2]’s and Rohwer *et al.* [17]’s E_p estimates significantly minimize uncertainties. In the case of Döll & Siebert [2], E_p values are often at the upper end of empirically determined efficiencies (Table S2, Fig. S6a–b). The same applies to Rohwer *et al.* [17], who compute E_p at the country level as a product of partial efficiencies,

$$E_p = E_a E_c M_f, \quad (5)$$

where E_a is the field application efficiency, E_c the conveyance efficiency and M_f a management factor. E_a and E_c are defined by the irrigation technology and M_f by the size of the irrigation system (Table S3).

The estimates provided by Rohwer *et al.* [17] leave some questions unanswered (Table S3). Firstly, their assignment of $E_a = 0.9$ to drip irrigation is based on a mechanistic understanding of irrigation technologies, as discussed in the Comment. Secondly, the use of $E_c = 0.95$ for sprinkler and drip irrigation presumes that these systems *are and remain* as efficient as lined, well-maintained channels, despite evidence indicating that poorly-maintained and operated drip systems may have no better efficiency than traditional surface systems [22]. Thirdly, the assignment of $M_f = 1$ and $M_f = 0.5$ to “small” ($< 10,000$ ha) and “large”

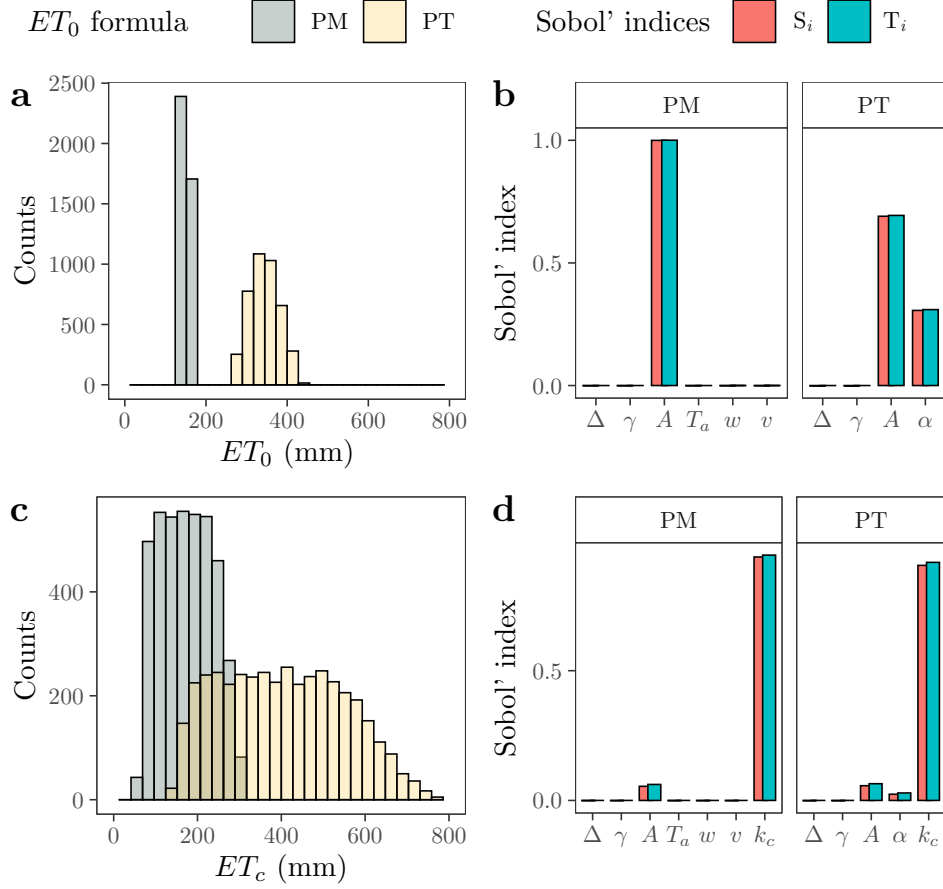


Figure S4: Variance-based global uncertainty and sensitivity analysis of the Penman-Monteith (PM, Equation 4) and the Priestley-Taylor (PT, Equation 3) methods. The red bars indicate the first-order effect S_i , i.e. the proportion of variance conveyed by each model input. The blue bars reflect the total-order effect T_i , which includes the first-order effect of the parameter plus the effect derived of its interaction with the rest. The uncertainty in the parameters is described with the probability distributions shown in Table S1. a) Distribution of ET_0 . b) Sobol' indices. c) Distribution of ET_c (Equation 2). We described the uncertainty in k_c as $\mathcal{U}(0.47, 1.86)$ to reproduce the range reported by Nichols *et al.* [13, Fig. 10] for developing salt cedars in the Bosque del Apache, New Mexico, in May (see Figure S5). d) Sobol' indices.

(> 10.000) irrigation systems contradicts Bos & Nugteren [21]'s data, which indicate an almost complete overlap in partial efficiencies between systems above and beyond 10.000 ha (Fig. S7). The selection of physical dimensions and the threshold of 10.000 ha to separate “small” from “large” irrigation systems appears to lack empirical support (Box 1).

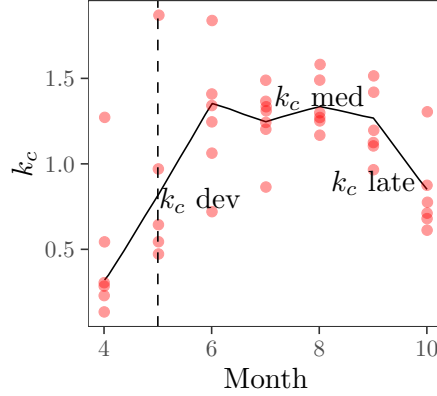


Figure S5: Evolution of k_c values for salt cedar. The solid black line is the mean k_c , the red dots show the individual measured values in the development, medium and late stage (adapted from Nichols *et al.* [13, Fig. 10]), and the vertical, dashed black line marks the values selected for the global sensitivity analysis presented in Figure S4c and d.

Box 1: Irrigated areas and scale

What is considered “large” or “small” is highly context-dependent. In Nepal the distinction between “small” and “large” systems varies depending not on their size but on their location, e.g. whether they are in flat (small < 500 ha, large > 5,000 ha) or non-flat (small < 50 ha, large > 5,00 ha) environments [23]. In Sri-Lanka, systems > 600 ha are considered “large”, those between 80-600 ha are regarded as “medium”, and those < 80 ha are considered “small” [24]. In India, “small” systems are those < 2,000 ha [25]; in Africa, those < 100 ha [26]. In al-Andalus (Spain, 8-15th centuries AD), irrigation systems below 1 ha were “small”, those between 1 and 2 were “medium-sized”, and those beyond 2 ha were “large” [27]. The conceptual ambiguity of the terms “small” and “large” is as well-known as their undue homogenization of irrigation systems with marked qualitative and quantitative differences [25, 28, 29].

If we compute E_p by letting E_a , E_c and M_f fluctuate over the empirical range reported by Bos & Nugteren [21] (Fig. S8), real-world uncertainties take center stage. Let’s focus on the irrigation efficiency of China, characterized by Rohwer *et al.* [17] with $E_a = 0.6$, $E_c = 0.7$, $M_f = 0.9$ and therefore $E_p = 0.38$. After a Monte-Carlo assessment of uncertainties, the E_p for China might be anywhere between 0.02 and 0.78 ($P_{2.5}, P_{97.5} = [0.1, 0.5]$), with E_a being responsible for most of the variance ($\sim 60\%$, Figure S9). If the uncertainty in the product $E_a E_c M_f$ is properly accounted for, the estimate provided by E_p may spread so much as to become of little help for policy-making.

Table S2: Comparison between the E_p values proposed by Döll & Siebert [2] for some regions and the E_p ranges documented in the studies which Döll & Siebert [2] use to justify their assignments.

Region	E_p	E_p range	Reference
United States	0.6	0.1–1 0.26–0.33	Solley <i>et al.</i> [18] (State level, Fig. S6a) Bos & Nugteren [21] (Project level)
South Asia	0.35	0.3–0.38 0.14–0.4	Guera <i>et al.</i> [19] (India) Bos & Nugteren [21] (India)
East Asia	0.35	0.11–0.34 0.22–0.33	Bos & Nugteren [21] (Japan) Bos & Nugteren [21] (Taiwan)
South-East Asia	0.4	0.4–0.65 0.35–0.45 0.37–0.62	Guera <i>et al.</i> [19] (Indonesia) Guera <i>et al.</i> [19] (Malaysia) Guera <i>et al.</i> [19] (Thailand)
Middle East	0.6	0.3 0.15 0.29	Bos & Nugteren [21] (Egypt) Bos & Nugteren [21] (Turkey) Bos & Nugteren [21] (Iran)
OECD Europe South	0.6	0.28–0.46 0.2–0.36 0.2–0.29 0.34 0.3	Bos & Nugteren [21] (France) Bos & Nugteren [21] (Greece) Bos & Nugteren [21] (Italy) Bos & Nugteren [21] (Portugal) Bos & Nugteren [21] (Spain)
OECD Europe North	0.5	0.41–0.57 0.07–0.6	Bos & Nugteren [21] (Netherlands) Bos & Nugteren [21] (Germany)
Northern Africa	0.7	0.45–0.8	FAO [20]
Western Africa	0.45	0.45–0.5	FAO [20]
Eastern Africa	0.55	0.45–0.8	FAO [20]
Southern Africa	0.55	0.5–0.65	FAO [20]

2 Uncertainty and sensitivity analysis

2.1 Variance-based sensitivity analysis

All the technical assessments of uncertainties and sensitivities conducted here and in the Comment are variance-based. Among the many sensitivity measures available, variance-based indices are considered best practice for they are model-free, global (they capture interactions) and easy to interpret. For a model of the form $y = f(\mathbf{x})$, $\mathbf{x} = (x_1, x_2, \dots, x_i, \dots, x_k) \in \mathbb{R}^k$, where y is a scalar and x_1, \dots, x_k are the k independent model inputs, the variance of y is decomposed into conditional terms as

$$V(y) = \sum_{i=1}^k V_i + \sum_i \sum_{i < j} V_{ij} + \dots + V_{1,2,\dots,k}, \quad (6)$$

Table S3: Comparison between the E_a, E_c , values proposed by Rohwer *et al.* [17] for surface, sprinkler and drip irrigation and the ranges documented by Bos & Nugteren [21] (in square brackets, see also Fig. S6c–d).

Efficiency	Surface	Sprinkler	Drip
E_a	0.6 [0.14–0.87]	0.75 [0.49–0.88]	0.9
E_c	0.7 [0.26–0.98]	0.95 [0.64–0.96]	0.95

where

$$V_i = V_{x_i} [E_{\mathbf{x}_{\sim i}}(y|x_i)] \quad V_{ij} = V_{x_i, x_j} [E_{\mathbf{x}_{\sim i, j}}(y|x_i, x_j)] \\ - V_{x_i} [E_{\mathbf{x}_{\sim i}}(y|x_i)] \\ - V_{x_j} [E_{\mathbf{x}_{\sim j}}(y|x_j)] \quad (7)$$

and so on up to the k -th order. The notation $\mathbf{x}_{\sim i}$ means *all-but- x_i* and $E(\cdot)$ is the mean operator. Note that Equation 6 is akin to Sobol’ [30]’s functional decomposition scheme:

$$f(\mathbf{x}) = f_0 + \sum_i f_i(x_i) + \sum_i \sum_{i < j} f_{ij}(x_i, x_j) + \dots + f_{1,2,\dots,k}(x_1, x_2, \dots, x_k), \quad (8)$$

where

$$f_0 = E(y) \quad f_i = E_{\mathbf{x}_{\sim i}}(y|x_i) - f_0 \quad f_{ij} = E_{\mathbf{x}_{\sim i, j}}(y|x_i, x_j) - f_i - f_j - f_0 \quad \dots, \quad (9)$$

and therefore

$$V_i = V[f_i(x_i)] \quad V_{ij} = V[f_{ij}(x_i, x_j)] \quad \dots, \quad (10)$$

and so on. Sobol’ [30] indices are then calculated as

$$S_i = \frac{V_i}{V(y)} \quad S_{ij} = \frac{V_{ij}}{V(y)} \quad \dots, \quad (11)$$

etc, where S_i is the first order effect of x_i on y , S_{ij} the second-order effect, and so forth. They can be expressed as the fractional reduction in the variance of y that may be obtained if x_i (x_i, x_j) could be fixed. In variance-based sensitivity analysis S_i is used to rank the model inputs in terms of their contribution to the model output variance, a setting known as “factor prioritization” [31].

By dividing all terms in Equation 6 by $V(y)$ we get

$$\sum_{i=1}^k S_i + \sum_i \sum_{i < j} S_{ij} + \dots + S_{1,2,\dots,k} = 1. \quad (12)$$

If $\sum_{i=1}^k S_i = 1$, the model is additive because all the model output variance can be decomposed as the sum of first-order effects. In other words, there are no interactions between the inputs. This is rarely the case in “real-life” models and often S_i is not enough to account for all the output variance.

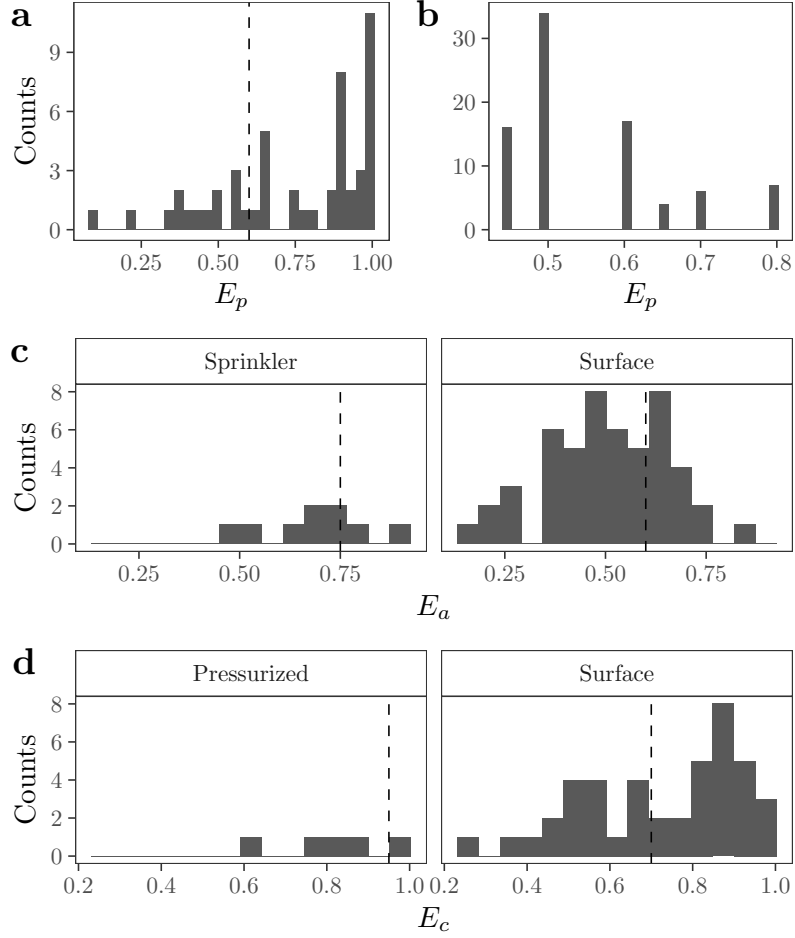


Figure S6: Data on irrigation efficiency. a) Distribution of project efficiencies (E_p) in USA according to Solley *et al.* [18], calculated as total water withdrawal / consumptive water use. The vertical dashed line is the E_p value used by Döll & Siebert [2] to characterize the irrigation efficiency of USA. b) Distribution of project efficiencies (E_p) for Africa reported by FAO [20]. c) Distribution of field application efficiencies (E_a) in surface and sprinkler irrigation systems according to Bos & Nugteren [21]. "Surface" includes furrow, basin and border irrigation systems. The dashed vertical lines mark the E_a point estimates selected by Rohwer *et al.* [17]. d) Distribution of conveyance efficiencies (E_c) in surface and pressurized (sprinkler) irrigation systems according to Bos & Nugteren [21]. The vertical, dashed black lines show the E_c point estimates used by Rohwer *et al.* [17].

In Equation 12 there are $2^k - 1$ terms. If the model under scrutiny has 10 parameters there would be 1,023 terms, making a full variance decomposition a very arduous task. To circumvent this issue Homma & Saltelli [32] proposed the total-order index T_i , which measures the first order effect of x_i jointly with its interactions with all the other inputs. It

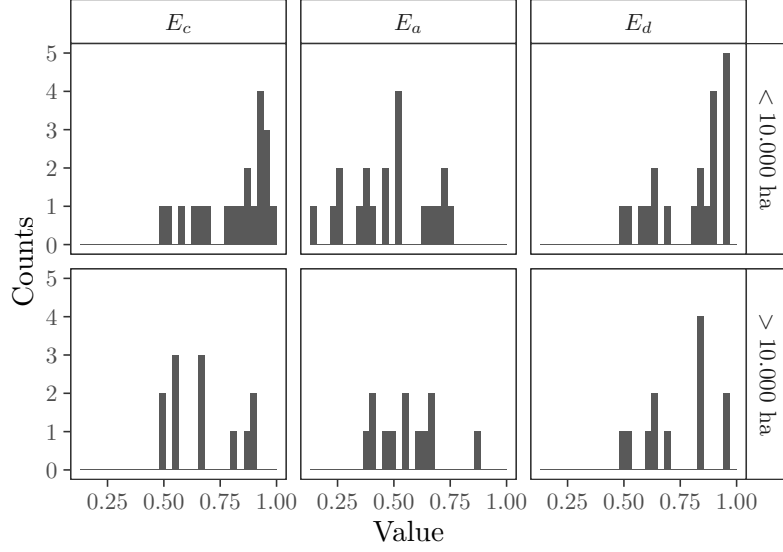


Figure S7: Partial efficiencies as a function of scale according to the data compiled by Bos & Nugteren [21]. E_d stands for distribution efficiency and refers to the water delivery from the source to a specific outlet. E_d is replaced by Rohwer *et al.* [17] with M_f .

is computed as

$$T_i = 1 - \frac{V_{\mathbf{x}_{\sim i}}[E_{x_i}(y|\mathbf{x}_{\sim i})]}{V(y)} = \frac{E_{\mathbf{x}_{\sim i}}[V_{x_i}(y|\mathbf{x}_{\sim i})]}{V(y)}. \quad (13)$$

When $T_i = 0$, then it can be concluded that x_i has no influence in the model output variance and thus can be fixed to any value within its uncertain range. T_i has been used to screen influential from non-influential parameters, a setting known as “factor fixing” [31].

2.2 Practical implementation

We first create a \mathbf{Q} matrix of row and column dimension N and $2k$ respectively, with k being the number of inputs of the model of interest, using Sobol’ [33] quasi-random numbers. We allocate the leftmost k columns to an \mathbf{A} matrix and the rightmost k columns to a \mathbf{B} matrix. These are the “base sample matrices”. Any point in \mathbf{A} or \mathbf{B} can be indicated as x_{vi} , where v indexes the row (from 1 to N) and i the column (from 1 to k). Then, k $\mathbf{A}_B^{(i)}$ matrices are created, where all columns come from \mathbf{A} except the i -th, which comes from \mathbf{B} . In these matrices each column is a model input whose uncertainty is described with the probability distribution that better matches the variability in the data.

The model runs rowwise over the \mathbf{A} , \mathbf{B} and $\mathbf{A}_B^{(i)}$ matrices for a total number of runs equal to $N_t = N(k + 2)$, and produces the vector of model outputs $\mathbf{y} = y_1, y_2, \dots, y_{N_t}$. We then compute S_i and T_i for all k model inputs using the Saltelli *et al.* [34] and the Jansen

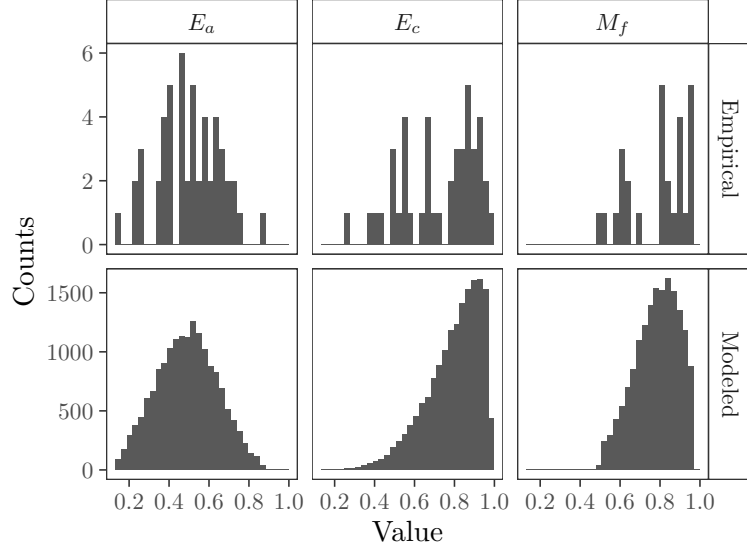


Figure S8: Empirical and modeled distributions for the uncertainty analysis conducted on the irrigation efficiencies of China. The data is based on Bos & Nugteren [21].

[35] estimators, which read as follows:

$$S_i = \frac{\frac{1}{N} \sum_{v=1}^N f(\mathbf{B})_v \left[f(\mathbf{A}_B^{(i)})_v - f(\mathbf{A})_v \right]}{V(y)} \quad (14)$$

$$T_i = \frac{\frac{1}{2N} \sum_{v=1}^N \left[f(\mathbf{A})_v - f(\mathbf{A}_B^{(i)})_v \right]^2}{V(y)} \quad (15)$$

We conduct all the uncertainty and sensitivity analysis (UA/SA) with the R package `sensobol` [36].

2.3 Assessment of uncertainties in the GHM literature

While sensitivity auditing has been largely missing from hydrological modeling (an exception being [37]), some studies have assessed quantifiable uncertainties. A survey of the literature reveals a clear preponderance of one-at-a-time (OAT) and piecewise approaches [38–42], which raise serious concerns on the reliability of the results.

Based on varying the parameter or structure of interest while all the other formative parts of the model are kept fixed, OAT’s capacity to explore the uncertainty space plummets as a function of the model dimensionality. This is consequence of the so-called “curse of dimensionality”, where every addition of a parameter leads to an exponential increase in the number of corners of the uncertainty space [34]. If the model is non-additive, then OAT also misses interactions, even at low dimensionality. Simple multiplications and divisions, let alone other mathematical operations, are enough to make a model non-additive.

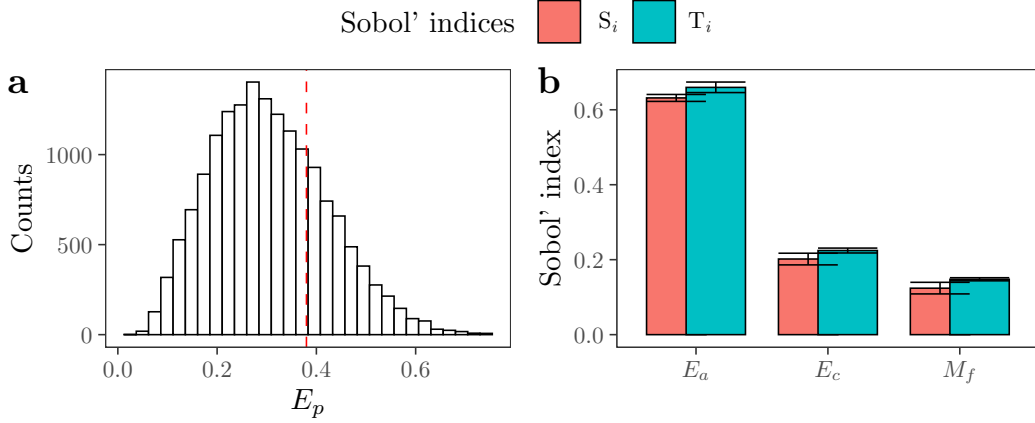


Figure S9: Uncertainty and sensitivity analysis of Equation 5. a) Empirical distribution of E_p for China once the uncertainties in E_a , E_c and M_f are accounted for based on the data by Bos & Nugteren [21]. The lack of correlations between them allow to treat E_a , E_c , M_f as independent parameters (Figure S12). The red, dashed line marks the E_p value assigned to China by Rohwer *et al.* [17]. b) Sobol' indices. For a description of the meaning of S_i and T_i , see Figure S4

For models with 2, 5 and 10 parameters, OAT can only examine 78%, 16% and 0.2% of the uncertainty space (Figure S10). If applied to higher-dimensional models (i.e. on ~ 20 parameters of WaterGap [43, 44]; on 38 parameters of PCR-GLOBWB [41]), the proportion of the input space explored becomes virtually indistinguishable from zero (2.4×10^{-6} and 8.3×10^{-18} respectively), and interaction effects are overlooked. Under these circumstances, the conclusions of an OAT analysis on a large-scale hydrological model are only reliable if the following assumptions hold: 1) the model has very few parameters, 2) the model behaves linearly or is at least additive, and 2) all effects take place in the minute portion of the input space explored, analogous to having found by chance a needle in a haystack.

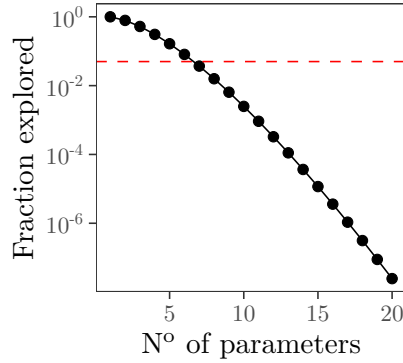


Figure S10: Fraction of the model input space explored with an OAT approach as a function of the model dimensionality k . The red, dashed line is at 0.05 (5%). See Saltelli & Annoni [45] for the technical details of the computation.

A piecewise sensitivity analysis breaks down the model uncertainty space into manageable units, either a few parameters and/or a few model structures, and investigates how their variation affects the model output (i.e. by changing the evaporation function in WBM [46], the selection of the irrigated area map and climate forcing in WBM_{plus} [39], the climate forcing, land cover input and model complexity in WaterGap [38], the hydraulic conductivity and river-bed conductance in PCR-GLOBWB [40]). If combined with an OAT [39, 40], this design misses not only the space formed by the factored-out parameters / structures, but also the space at the intersection between those factored in and between those factored in *and* out. The use of multi-model ensembles (i.e. [47, 48]) as a way to treat uncertainties is a piecewise approach all the same: models are treated like isolated compartments and hence the interactions between parametric and structural uncertainties within models are left untouched.

2.4 One-at-a-time (OAT) approach

In section 2.5 we also perform a one-at-a-time (OAT) analysis to show the limitations of this method in exploring the model’s uncertainty space. For this design, we construct $k \mathbf{A}_{\sim i}$ matrices, where all model inputs except the i -th are fixed to their nominal values and the i -th varies along its uncertainty range.

2.5 Uncertainty and sensitivity analysis at the grid cell level

Here we describe the rationale of the uncertainty analysis in the paragraph ”Extent of Uncertainties” of the Comment, where we examine how large the uncertainty in the irrigation water withdrawal estimates can get once all the main uncertainties at the grid cell level are properly factored in. We also provide the results of the sensitivity analysis, which is missing from the Comment due to space restrictions.

We focus on a specific grid cell in the Uvalde County, Texas, United States of America ($x = -99.7084$, $y = 29.4583$), for the following reasons:

- The availability of empirical k_c data. Ko *et al.* [49] produced several growth-stage-specific k_c values for wheat (*Triticum aestivum*) in an empirical study conducted at the Texas AgriLife Research field, Uvalde (November 2006 – May 2007). We focus on the period January 6–7 2007, approximately 50–52 days after planting. We assume that wheat is the only crop grown in the grid cell considered. Simplifications as such are common in large-scale hydrological models: for instance, WaterGap classifies all crops in all cells as either rice or non-rice [50]. In our case, the assumption that the entire cell considered is planted with wheat does not affect the main goal of the analysis, which is to show how previous approaches to uncertainties are perfunctory.
- The availability of data for the extension of irrigation. At $x = -99.7084$, $y = 29.4583$, the GRIPC [6] and the FAO-GMIA [10] respectively report irrigated areas of 42.9 ha and 144.5 ha. The map by Meier *et al.* [7] and the IWMI-GIAM [5] have a different resolution and do not produce any data for this specific coordinate. The closest cell in the Meier map is located at $x = -99.70416$, $y = 29.44834$, 12.5 km to the south, and reports an irrigated area of 75 ha.

- The availability of empirical data to characterize the climatic and environmental parameters in ET_0 on a daily basis in Uvalde for the period of interest. We extract the information from <https://www.wunderground.com/history/daily/KUVA/date/2003-1-1>. This link was accessed February 23 2021.

We briefly recall the equation to compute irrigation water withdrawals, which we write as

$$y = \frac{I_a \left[k_c \frac{0.408\Delta A + \gamma \frac{900}{T_a + 273} wv}{\Delta + \gamma(1 + 0.34w)} - P \right]}{(E_a E_c M_f)} \quad (16)$$

where y is the water withdrawn for irrigation. Note that we use the Priestley-Taylor formula for ET_0 and Rohwer *et al.* [17]’s approach to E_p and hence we are waving important structural uncertainties to keep the analysis simple. Equation 16 has twelve parameters, whose uncertainties are described with the probability distributions in Table S4.

Table S4: Summary of the uncertainty in the parameters.

N°	Input	Description	Distribution
1	Δ	Vapour pressure	$\mathcal{U}(0.0796, 0.0804)$
2	γ	Psychrometric constant	$\mathcal{U}(0.065, 0.066)$
3	A	Net radiation minus soil heat flux	$\mathcal{U}(297.550, 402.448)$
4	T_a	Mean air temperature	$\mathcal{U}(9.9, 10.1)$
5	w	Wind speed	$\mathcal{U}(2.67, 2.95)$
6	v	Vapor deficit	$\mathcal{U}(0.26, 0.29)$
7	k_c	Crop coefficient	$\mathcal{U}(0.45, 1.14)$
8	I_a	Irrigated area	$\mathcal{U}(42.9, 144.5)$
9	E_a	Field application efficiency	$\mathcal{U}(0.49, 0.88)$
10	E_c	Conveyance efficiency	$\mathcal{U}(0.64, 0.96)$
11	M_f	Management factor	$\mathcal{U}(0.50, 0.97)$
12	P	Precipitation	$\mathcal{U}(0, 0.1)$

The first six parameters in Table S4 are needed to compute ET_0 following the FAO-56 Penman-Monteith formula. The uncertainties reflect the manufacturer’s estimates of the errors in the instruments used by Nichols *et al.* [13] and his work in the Bosque del Apache region. We assume that these error estimates can be extrapolated to the devices used to record the data in Uvalde too.

We calculate the value of these parameters based on the mean air temperature (T_a) in Uvalde between January 6-7 2007. Vapor pressure (Δ) is computed as

$$\Delta = \frac{4098 e_{sat}}{(T_a + 237.3)^2}, \quad (17)$$

where e_{sat} is the Tetens equation for saturation vapor pressure, calculated as

$$e_{sat} = 0.6108 \exp \left[\frac{17.27 T_a}{(T_a + 237.3)} \right]. \quad (18)$$

We estimate the vapor deficit (v) as

$$v = e_{sat} - e_{sat} h_{rel}, \quad (19)$$

where $h_{rel} = 0.77$, the mean relative humidity in Uvalde during the period of interest. As for the psychrometric constant (γ), it is calculated as

$$\gamma = 0.0016286 \frac{p}{\lambda}, \quad (20)$$

where λ is the latent heat of vaporization, estimated as

$$\lambda = 2.501 - 0.002361 T_a, \quad (21)$$

and p is the atmospheric pressure, calculated as

$$p = 101.3 \left[\frac{293 - 0.0065z}{293} \right]^{5.256}, \quad (22)$$

where $z = 9$, the height (m) above ground where air measurements are made.

We describe k_c as $k_c \sim \mathcal{U}(0.45, 1.14)$ following the k_c coefficients available for January 6–7 2007 (Fig. S11).

The irrigated area is characterized as $I_a \sim \mathcal{U}(42.9, 144.5)$, i.e. with the upper and lower bounds for the extension of irrigation documented by the GRIPC [6], the FAO-GMIA [10] and the Meier map [7]. We assume that any size between these bounds is equally possible.

As for E_a and E_c , we describe them as $E_a \sim \mathcal{U}(0.49, 0.88)$ and $E_c \sim \mathcal{U}(0.64, 0.96)$ following the data retrieved by Bos & Nugteren [21] for sprinkler irrigation (Fig. S6c, d). Rohwer *et al.* [17, Annex B] assign United States to the sprinkler category according to their decision tree. With regards to the management factor, we characterize it as $M_f \sim \mathcal{U}(0.5, 0.97)$ following the range reported by Bos & Nugteren [21], which does not allow to substantiate any significant difference between systems above and below 10,000 ha (Fig. S7).

In our Monte-Carlo analysis we consider E_a, E_c, M_f to be independent as there is no evidence of them being correlated (Figure S12).

Finally, we describe P as $P \sim \mathcal{U}(0, 0.1)$ following the precipitation rates attested in Uvalde between January 6–7 2007.

The results of the global uncertainty and sensitivity analysis are displayed in Figure S13. If the computation is done with point estimates for each parameter (i.e. their nominal values), $y = 270,000 \text{ m}^3$. This is the methodology adopted by large-scale hydrological models, which output scalar values for each grid cell. With an OAT-based approach we obtain the range 170,000–370,000 $\text{m}^3 \text{ ha d}^{-1}$ ($P_{2.5}, P_{97.5}$), whereas a complete exploration of the uncertainty space by means of a global sensitivity analysis widens the range to 90,000–670,000 m^3 ($P_{2.5}, P_{97.5}$), with the right tail pushing estimates up to 1,220,000 m^3 (Figure S13a). The uncertainty thus spans about one and a half orders of magnitude and is more than two times larger than the range yielded by an OAT design. It is also worth noting that interactions between E_a, E_c, I_a, k_c, M_f explain c. 10% of the model output variance, with several second-order effects that would have passed undetected with an OAT (Figure S13b–c).

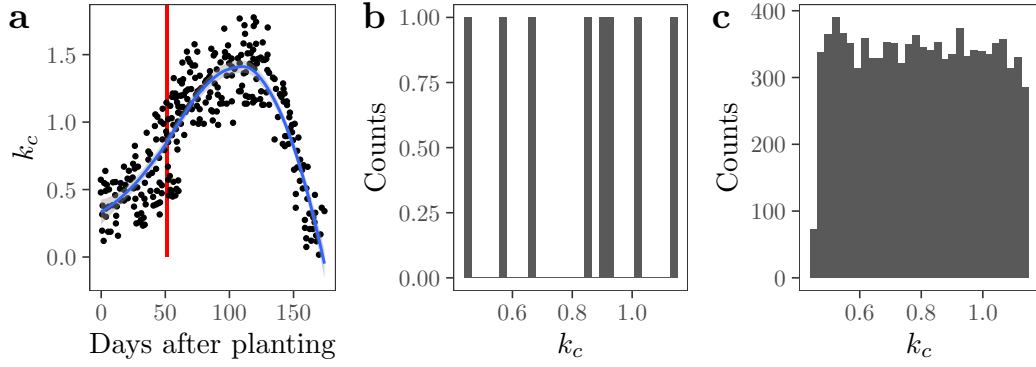


Figure S11: k_c coefficients for *Triticum aestivum* (wheat). a) Estimated k_c coefficients. The blue line shows the smoothed mean, whereas the red vertical line marks the wheat development period examined for the uncertainty and sensitivity analysis considered here. Data retrieved from Ko *et al.* [51, Figure 3]. b) Empirical distribution of k_c coefficients for wheat during the selected period. c) Uniform distribution modeled after b).

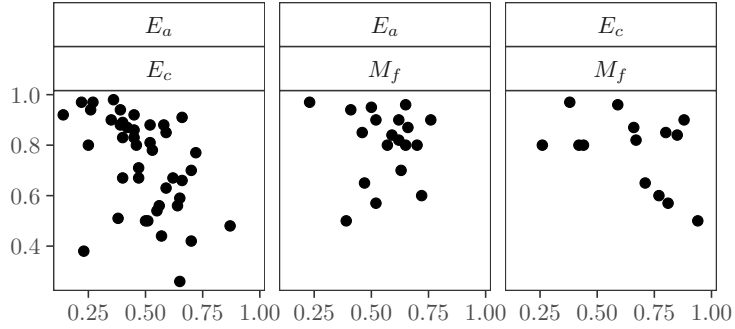


Figure S12: Scatterplots of E_a, E_c, M_f . The topmost and bottommost label facets refer to the x and the y axis respectively.

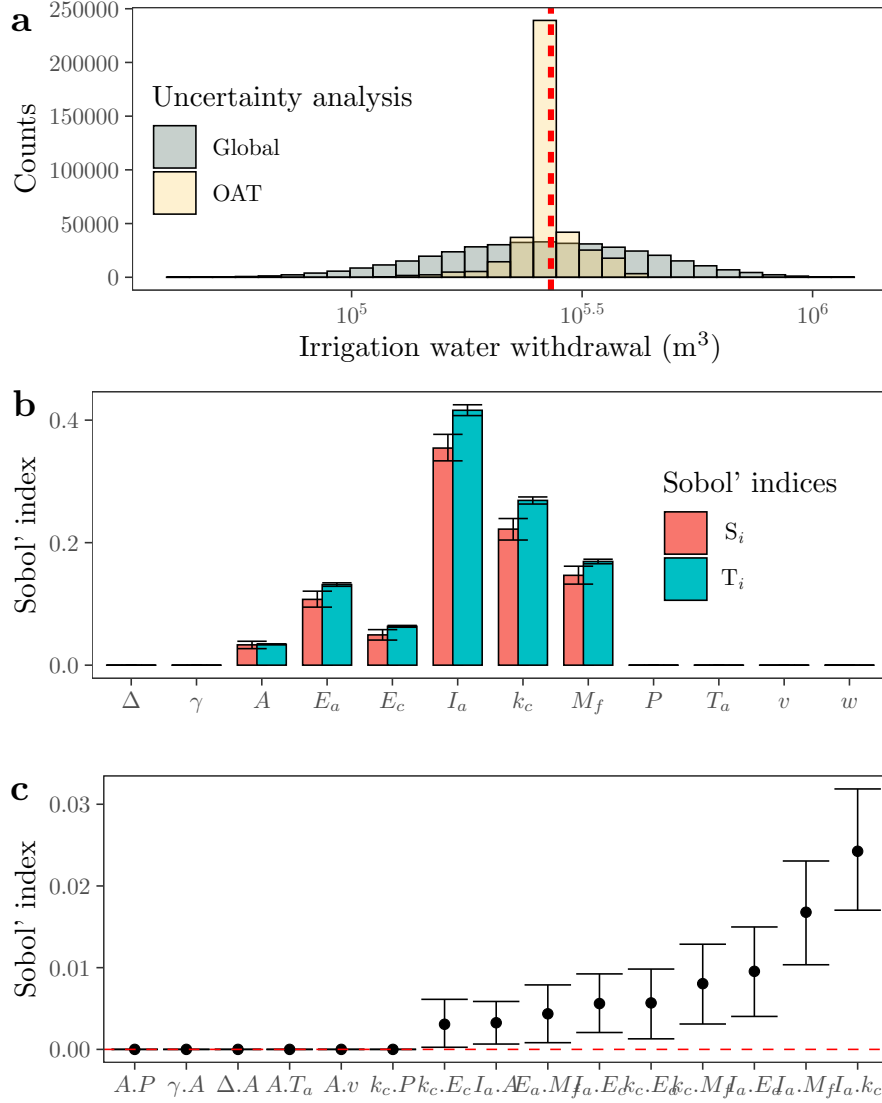


Figure S13: Comparison between an OAT and a global-sensitivity analysis of Equation 16. a) Uncertainty analysis. The thick, red dashed line shows the point estimate obtained after computing Equation 16 using the mean value of the parameters, equivalent to what large-scale hydrological models do at the grid cell level (use of point-estimates). b) Sobol' indices. The red bar indicates the first-order effect S_i , i.e. the proportion of variance conveyed by each model input. The blue bar reflects the total-order effect T_i , which includes the first-order effect of the parameter plus the effect derived of its interaction with the rest. The parameters were described with the probability distributions shown in Table S4. c) Significant second-order effects. The error bars reflect the 95% confidence intervals, computed with the normal method after bootstrapping the indices 10^3 times.

References

1. Wada, Y., Flörke, M., Hanasaki, N., Eisner, S., Fischer, G., Tramberend, S., Satoh, Y., Van Vliet, M. T., Yillia, P., Ringler, C., Burek, P. & Wiberg, D. Modeling global water use for the 21st century: The Water Futures and Solutions (WFaS) initiative and its approaches. *Geoscientific Model Development* **9**, 175–222. doi:[10.5194/gmd-9-175-2016](https://doi.org/10.5194/gmd-9-175-2016) (2016).
2. Döll, P. & Siebert, S. Global modeling of irrigation water requirements. *Water Resources Research* **38**, 8–1–8–10. doi:[10.1029/2001WR000355](https://doi.org/10.1029/2001WR000355) (2002).
3. Jackson, R. B., Canadell, J., Ehleringer, J. R., Mooney, H. A., Sala, O. E. & Schulze, E. D. A global analysis of root distributions for terrestrial biomes. *Oecologia* **108**, 389–411. doi:[10.1007/BF00333714](https://doi.org/10.1007/BF00333714) (1996).
4. Siebert, S., Döll, P., Hoogeveen, J., Faures, J.-M., Frenken, K. & Feick, S. Development and validation of the global map of irrigation areas. *Hydrology and Earth System Sciences* **9**, 535–547. doi:[10.5194/hess-9-535-2005](https://doi.org/10.5194/hess-9-535-2005) (Nov. 2005).
5. Thenkabail, P. S., Biradar, C. M., Noojipady, P., Dheeravath, V., Li, Y., Velpuri, M., Gumma, M., Gangalakunta, O. R. P., Turrall, H., Cai, X., Vithanage, J., Schull, M. & Dutta, R. Global irrigated area map (GIAM), derived from remote sensing, for the end of the last millennium. *International Journal of Remote Sensing* **30**, 3679–3733. doi:[10.1080/01431160802698919](https://doi.org/10.1080/01431160802698919) (2009).
6. Salmon, J., Friedl, M. A., Frohling, S., Wisser, D. & Douglas, E. M. Global rain-fed, irrigated, and paddy croplands: A new high resolution map derived from remote sensing, crop inventories and climate data. *International Journal of Applied Earth Observation and Geoinformation* **38**, 321–334. doi:[10.1016/j.jag.2015.01.014](https://doi.org/10.1016/j.jag.2015.01.014) (2015).
7. Meier, J., Zabel, F. & Mauser, W. A global approach to estimate irrigated areas. A comparison between different data and statistics. *Hydrology and Earth System Sciences* **22**, 1119–1133. doi:[10.5194/hess-22-1119-2018](https://doi.org/10.5194/hess-22-1119-2018) (2018).
8. FAO. *AQUASTAT website* 2016.
9. FAO. *FAOSTAT database* Rome, 2017.
10. Siebert, S., Henrich, V., Frenken, K. & Burke, J. *Update of the digital global map of irrigation areas to version 5* Bonn, Rome, 2013. doi:[10.13140/2.1.2660.6728](https://doi.org/10.13140/2.1.2660.6728).
11. McMahon, T. A., Peel, M. C., Lowe, L., Srikanthan, R. & McVicar, T. R. Estimating actual, potential, reference crop and pan evaporation using standard meteorological data: A pragmatic synthesis. *Hydrology and Earth System Sciences* **17**, 1331–1363. doi:[10.5194/hess-17-1331-2013](https://doi.org/10.5194/hess-17-1331-2013) (2013).
12. Allen, R. G., Pereira, L. S., Raes, D. & Smith, M. Crop evapotranspiration (guidelines for computing crop water requirements). *Irrigation and Drainage* **300**, 300 (1998).
13. Nichols, J., Eichinger, W., Cooper, D. I., Prueger, J. H., Hipps, L. E., Neale, C. M. U. & Bawazir, A. S. *Comparison of Evaporation Estimation Methods for a Riparian Area. Final report* tech. rep. 436 (IIHR - Hydroscience & Engineering, College of Engineering, University of Iowa, Iowa City, 2004).

14. Multsch, S., Exbrayat, J. F., Kirby, M., Viney, N. R., Frede, H. G. & Breuer, L. Reduction of predictive uncertainty in estimating irrigation water requirement through multi-model ensembles and ensemble averaging. *Geoscientific Model Development* **8**, 1233–1244. doi:[10.5194/gmd-8-1233-2015](https://doi.org/10.5194/gmd-8-1233-2015) (2015).
15. Dessai, S. & van der Sluijs, J. *Modelling Climate Change Impacts for Adaptation Assessments* (eds Christie, M., Cliffe, A., Dawid, P. & Senn, S.) 83–102 (Wiley, Chichester, UK, 2011).
16. Halsnæs, K. & Kaspersen, P. S. Decomposing the cascade of uncertainty in risk assessments for urban flooding reflecting critical decision-making issues. *Climatic Change* **151**, 491–506. doi:[10.1007/s10584-018-2323-y](https://doi.org/10.1007/s10584-018-2323-y) (2018).
17. Rohwer, J., Gerten, D. & Lucht, W. Development of functional irrigation types for improved global crop modelling. *PIK Report*, 1–61 (2007).
18. Solley, W. B., Pierce, R. R. & Perlman, H. *Estimated Use of Water in the United States in 1995* tech. rep. (US Geological Survey Circular 1200, 1998), 50.
19. Guera, L. C., Bhuiyan, S. I., Tuong, T. P. & Barker, R. *Producing More Rice with Less Water from irrigated Systems* tech. rep. (International Rice Research Institute, Manila, 1998).
20. FAO. *Irrigation Potential in Africa. A Basin Approach. FAO Land and Water Bulletin 4* tech. rep. (Food and Agriculture Organization of the United Nations, Rome, 1997).
21. Bos, M. & Nugteren, J. *On Irrigation Efficiencies* tech. rep. (International Institute for Land Recamation and Improvement / ILRI, Wageningen, 1990).
22. Wolf, J. M., Gleason, J. E. & Hagan, R. E. *Proceedings of the 1995 Water Management Seminar, Irrigation Conservation Opportunities and Limitations* 209–217 (US Committee on Irrigation and Drainage, Sacramento, 1995).
23. Lam, W. F. Improving the performance of small-scale irrigation systems: the effects of technological investments and governance structure on irrigation performance in Nepal. *World Development* **24**, 1301–1315. doi:[10.1016/0305-750X\(96\)00043-5](https://doi.org/10.1016/0305-750X(96)00043-5) (Aug. 1996).
24. Murray, F. J. & Little, D. C. *The Nature of Small-Scale Farmer Managed Irrigation Systems In North West Province, Sri Lanka, and Potential for Aquaculture*. tech. rep. (UK Department for International Development (DFID) R7064, 2000).
25. Vincent, L. Lost chances and new futures. Interventions and institutions in small-scale irrigation. *Land Use Policy* **11**, 309–322 (1994).
26. FAO. *Irrigation and Drainage. Paper 48* tech. rep. (FAO, Rome, 1987).
27. Sitjes, E. Inventario y tipología de sistemas hidráulicos de Al-Andalus. *Arqueología Espacial* **26**, 263–292 (2006).
28. Carter, R. C. & Howsam, P. Sustainable use of groundwater for smallscale irrigation: With special reference to sub-Saharan Africa. *Land Use Policy* **11**, 275–285 (1994).
29. Guijt, I. & Thompson, J. Landscapes and livelihoods. Environmental and socio-economic dimensions of small-scale irrigation. *Land Use Policy* **11**, 294–308 (1994).

30. Sobol', I. M. Sensitivity analysis for nonlinear mathematical models. *Mathematical Modeling and Computational Experiment* **1**, 407–414 (1993).
31. Saltelli, A., Ratto, M., Andres, T., Campolongo, F., Cariboni, J., Gatelli, D., Saisana, M. & Tarantola, S. *Global Sensitivity Analysis. The Primer* doi:[10.1002/9780470725184](https://doi.org/10.1002/9780470725184) (John Wiley & Sons, Ltd, Chichester, UK, Dec. 2008).
32. Homma, T. & Saltelli, A. Importance measures in global sensitivity analysis of nonlinear models. *Reliability Engineering & System Safety* **52**, 1–17. doi:[10.1016/0951-8320\(96\)00002-6](https://doi.org/10.1016/0951-8320(96)00002-6) (Apr. 1996).
33. Sobol', I. M. On the distribution of points in a cube and the approximate evaluation of integrals. *USSR Computational Mathematics and Mathematical Physics* **7**, 86–112. doi:[10.1016/0041-5553\(67\)90144-9](https://doi.org/10.1016/0041-5553(67)90144-9) (Jan. 1967).
34. Saltelli, A., Annoni, P., Azzini, I., Campolongo, F., Ratto, M. & Tarantola, S. Variance based sensitivity analysis of model output. Design and estimator for the total sensitivity index. *Computer Physics Communications* **181**, 259–270. doi:[10.1016/j.cpc.2009.09.018](https://doi.org/10.1016/j.cpc.2009.09.018) (Feb. 2010).
35. Jansen, M. Analysis of variance designs for model output. *Computer Physics Communications* **117**, 35–43. doi:[10.1016/S0010-4655\(98\)00154-4](https://doi.org/10.1016/S0010-4655(98)00154-4) (Mar. 1999).
36. Puy, A., Lo Piano, S., Saltelli, A. & Levin, S. A. sensobol: an R package to compute variance-based sensitivity indices. *Journal of Statistical Software*. arXiv: [2101.10103](https://arxiv.org/abs/2101.10103) (2022).
37. Peeters, L. J. Assumption hunting in groundwater modeling: find assumptions before they find you. *Groundwater* **55**, 665–669. doi:[10.1111/gwat.12565](https://doi.org/10.1111/gwat.12565) (2017).
38. Müller Schmied, H., Eisner, S., Franz, D., Wattenbach, M., Portmann, F. T., Flörke, M. & Döll, P. Sensitivity of simulated global-scale freshwater fluxes and storages to input data, hydrological model structure, human water use and calibration. *Hydrology and Earth System Sciences* **18**, 3511–3538. doi:[10.5194/hess-18-3511-2014](https://doi.org/10.5194/hess-18-3511-2014) (2014).
39. Wisser, D., Froking, S., Douglas, E. M., Fekete, B. M., Vörösmarty, C. J. & Schumann, A. H. Global irrigation water demand: Variability and uncertainties arising from agricultural and climate data sets. *Geophysical Research Letters* **35**, 1–5. doi:[10.1029/2008GL035296](https://doi.org/10.1029/2008GL035296) (2008).
40. De Graaf, I. E. M., Gleeson, T., (Rens) van Beek, L. P. H., Sutanudjaja, E. H. & Bierkens, M. F. P. Environmental flow limits to global groundwater pumping. *Nature* **574**, 90–94. doi:[10.1038/s41586-019-1594-4](https://doi.org/10.1038/s41586-019-1594-4) (2019).
41. Sperna Weiland, F. C., Vrugt, J. A., van Beek, R. L., Weerts, A. H. & Bierkens, M. F. Significant uncertainty in global scale hydrological modeling from precipitation data errors. *Journal of Hydrology* **529**, 1095–1115. doi:[10.1016/j.jhydro.2015.08.061](https://doi.org/10.1016/j.jhydro.2015.08.061) (2015).
42. Wada, Y., Wisser, D. & Bierkens, M. F. P. Global modeling of withdrawal, allocation and consumptive use of surface water and groundwater resources. *Earth System Dynamics* **5**, 15–40. doi:[10.5194/esd-5-15-2014](https://doi.org/10.5194/esd-5-15-2014) (2014).

43. Schumacher, M., Eicker, A., Kusche, J., Müller Schmied, H. & Döll, P. *Covariance Analysis and Sensitivity Studies for GRACE Assimilation into WGHM IAG Symposia Series: Proceedings of the IAG Scientific Assembly 2013* (2015), 241–247. doi:[10.1007/1345](https://doi.org/10.1007/1345).
44. Werth, S. & Güntner, A. Calibration analysis for water storage variability of the global hydrological model WGHM. *Hydrology and Earth System Sciences* **14**, 59–78 (2010).
45. Saltelli, A. & Annoni, P. How to avoid a perfunctory sensitivity analysis. *Environmental Modelling and Software* **25**, 1508–1517. doi:[10.1016/j.envsoft.2010.04.012](https://doi.org/10.1016/j.envsoft.2010.04.012) (2010).
46. Vörösmarty, C. J., Federer, C. A. & Schloss, A. L. Potential evaporation functions compared on US watersheds: Possible implications for global-scale water balance and terrestrial ecosystem modeling. *Journal of Hydrology* **207**, 147–169. doi:[10.1016/S0022-1694\(98\)00109-7](https://doi.org/10.1016/S0022-1694(98)00109-7) (1998).
47. Wada, Y., Wisser, D., Eisner, S., Flörke, M., Gerten, D., Haddeland, I., Hanasaki, N., Masaki, Y., Portmann, F. T., Stacke, T., Tessler, Z. & Schewe, J. Multimodel projections and uncertainties of irrigation water demand under climate change. *Geophysical Research Letters* **40**, 4626–4632. doi:[10.1002/grl.50686](https://doi.org/10.1002/grl.50686) (2013).
48. Bierkens, M. F. P. Global hydrology 2015: State, trends, and directions. *Water Resources Research* **51**, 4923–4947. doi:[10.1002/2015WR017173](https://doi.org/10.1002/2015WR017173) (July 2015).
49. Ko, J., Piccinni, G., Marek, T. & Howell, T. Determination of growth-stage-specific crop coefficients (Kc) of cotton and wheat. *Agricultural Water Management* **96**, 1691–1697. doi:[10.1016/j.agwat.2009.06.023](https://doi.org/10.1016/j.agwat.2009.06.023) (2009).
50. Müller Schmied, H., Caceres, D., Eisner, S., Flörke, M., Herbert, C., Niemann, C., Asali Peiris, T., Popat, E., Theodor Portmann, F., Reinecke, R., Schumacher, M., Shadkam, S., Telteu, C. E., Trautmann, T. & Döll, P. The global water resources and use model WaterGAP v2.2d: Model description and evaluation. *Geoscientific Model Development* **14**, 1037–1079. doi:[10.5194/gmd-14-1037-2021](https://doi.org/10.5194/gmd-14-1037-2021) (2021).
51. Ko, J., Piccinni, G., Marek, T. & Howell, T. Determination of growth-stage-specific crop coefficients (Kc) of cotton and wheat. *Agricultural Water Management* **96**, 1691–1697. doi:[10.1016/j.agwat.2009.06.023](https://doi.org/10.1016/j.agwat.2009.06.023) (2009).